A polarized positron beam for DVCS on the proton with CLAS12 at Jefferson Lab

Volker D. Burkert[1,a)], L. Elouadrhiri[1] and F.-X. Girod[1]

[1]*Jefferson Laboratory, 12000 Jefferson Avenue, Newport News, Virginia, 23606*

[a)]Corresponding author: burkert@jlab.org

Abstract. The measurement of Deeply Virtual Compton Scattering on the proton with a polarized positron beam in CLAS12 can give access to a complete set of observables for the extraction of Generalized Parton Distributions with the upgraded 11-GeV CEBAF. This provides a clean separation of the real and imaginary parts of the amplitudes, greatly simplifies the analysis, and provides a crucial handle on the model dependences and associated systematic uncertainties. The real part of the amplitude is in particular sensitive to the D-term which parameterizes the Gravitational Form Factors of the nucleon. Azimuthal Dependences and t-dependences of the Azimuthal Moments for Beam Charge Asymmetries on unpolarized Hydrogen are estimated using a 1000 hours run with a luminosity of 2×10^{34} cm^{-2}s^{-1} and 80% beam polarization.

INTRODUCTION

The challenge of understanding nucleon electromagnetic structure still continues after six decades of experimental scrutiny. From the initial measurements of elastic form factors to the accurate determination of parton distributions through deep inelastic scattering, the experiments have increased in statistical and systematic accuracy. During the past two decades it was realized that the parton distribution functions represent special cases of a more general, much more powerful, way to characterize the structure of the nucleon, the generalized parton distributions (GPDs) (see [1, 28] for reviews).

The GPDs are the Wigner quantum phase space distribution of quarks in the nucleon describing the simultaneous distribution of particles with respect to both position and momentum in a quantum-mechanical system. In addition to the information about the spatial density and momentum density, these functions reveal the correlation of the spatial and momentum distributions, *i.e.* how the spatial shape of the nucleon changes when probing quarks of different momentum fraction of he nucleon.

The concept of GPDs has led to completely new methods of "spatial imaging" of the nucleon in the form of (2+1)-dimensional tomographic images, with 2 spatial dimensions and 1 dimension in momentum [3, 4, 5]. The second moments of GPDs are related to form factors that allow us to quantify how the orbital motion of quarks in the nucleon contributes to the nucleon spin, and how the quark masses and the forces on quarks are distributed in transverse space, a question of crucial importance for our understanding of the dynamics underlying nucleon structure and the forces leading to color confinement.

The four leading twist GPDs H, $\tilde{H}$, E, and $\tilde{E}$, depend on the 3 variable x, ξ, and t, where x is the longitudinal momentum fraction of the struck quark, ξ is the longitudinal momentum transfer to the quark ($\xi \approx x_B/(2 - x_B)$), and t is the invariant 4-momentum transfer to the proton. The mapping of the nucleon GPDs, and a detailed understanding of the spatial quark and gluon structure of the nucleon, have been widely recognized as key objectives of nuclear physics of the next decades. This requires a comprehensive program, combining results of measurements of a variety of processes in electron–nucleon scattering with structural information obtained from theoretical studies, as well as with expected results from future lattice QCD simulations. The `CLAS12` detector, shown in Fig. 2, has recently been completed and has begun the experimental science program in the 12 GeV era Jefferson Lab.

ACCESSING GPD IN DVCS

The most direct way of accessing GPDs at lower energies is through the measurement of Deeply Virtual Compton Scattering (DVCS) in a kinematical domain where the so-called handbag diagram shown in Fig. 1 makes the dominant contributions. However, in DVCS as in other deeply virtual reactions, the GPDs do not appear directly in the cross section, but in convolution integrals called Compton Form Factors (CFF), which are complex quantities defined as, e.g. fro GPD H:

$$\mathcal{H}(\xi,t) \equiv \int_{-1}^{+1} \frac{H^q(x,\xi,t)dx}{x-\xi+i\epsilon} = \int_{-1}^{+1} \frac{H^q(x,\xi,t)dx}{x-\xi} + i\pi H^q(\xi,\xi,t)\,, \tag{1}$$

where the first term on the r.h.s. corresponds to the real part and the second term to the imaginary part of the scattering amplitude. The superscript q indicates that GPDs depend on the quark flavor. From the above expression it is obvious that GPDs, in general, can not be accessed directly in measurements. However, in some kinematical regions the Bethe-Heitler (BH) process where high energy photons are emitted from the incoming and scattered electrons, can be important. Since the BH amplitude is purely real, the interference with the DVCS amplitude isolates the imaginary part of the DVCS amplitude. The interference of the two processes offers the unique possibility to determine GPDs directly at the singular kinematics $x = \xi$. At other kinematical regions a deconvolution of the cross section is required to determine the kinematic dependencies of the GPDs. It is therefore important to obtain all possible independent information that will aid in extracting information on GPDs. The interference terms for polarized beam I_{LU}, longitudinally polarized target I_{UL}, transversely (in scattering plane) polarized target I_{UT}, and perpendicularly (to scattering plane) polarized target I_{UP} are given by the expressions:

$$I_{LU} \sim \sqrt{\tau'}[F_1 H + \xi(F_1+F_2)\tilde{H} + \tau F_2 E] \tag{2}$$

$$I_{UL} \sim \sqrt{\tau'}[F_1 \tilde{H} + \xi(F_1+F_2)H + (\tau F_2 - \xi F_1)\xi\tilde{E}] \tag{3}$$

$$I_{UP} \sim \tau[F_2 H - F_1 E + \xi(F_1+F_2)\xi\tilde{E} \tag{4}$$

$$I_{UT} \sim \tau[F_2 \tilde{H} + \xi(F_1+F_2)E - (F_1+\xi F_2)\xi\tilde{E}] \tag{5}$$

where $\tau = -t/4M^2$, $\tau' = (t_0 - t)/4M^2$. By measuring all 4 combinations of interference terms one can separate all 4 leading twist GPDs at the specific kinematics $x = \xi$. Experiments at JLab using 4 to 6 GeV electron beams have been carried out with polarized beams [34, 7, 33, 9, 10] and with longitudinal target [11, 12, 13], showing the feasibility of such measurements at relatively low beam energies, and their sensitivity to the GPDs. Techniques of how to extract GPDs from existing DVCS data and what has been learned about GPDs can be found in [37, 15]. In the following sections we discuss what information may be gained by employing both electron and positron beams in deeply virtual photon production.

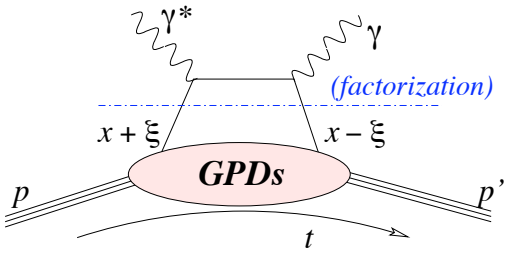

FIGURE 1. Leading order contributions to the production of high energy single photons from protons. The DVCS handbag diagram contains the information on the unknown GPDs.

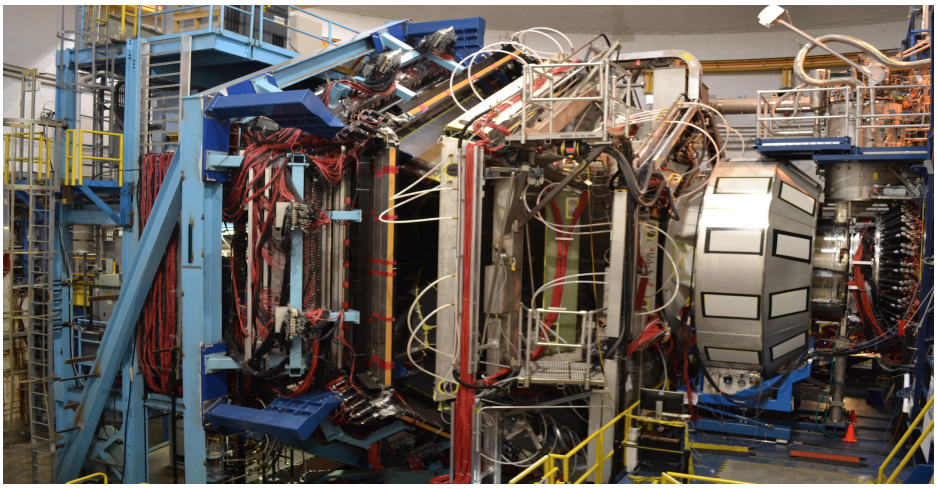

FIGURE 2. The CLAS12 detector in Hall B. The beam line is running from the right to the left. The liquid hydrogen target is centered in the solenoid magnet with 5 Tesla central magnetic field, and is surrounded by tracking and particle identification detectors covering and polar angle range from 40° to 125°. The forward detector consists of the 2π gas Cherenkov Counter (large silvery box to the right), the tracking chambers around the superconducting Torus magnet, 2 layers of time-of-flight systems and two layers of electromagnetic calorimeters for electron triggering and photon detection to the far left.

Differential cross section for polarized electrons and positrons

The structure of the differential cross section for polarized beam and unpolarized target is given by:

$$\sigma_{\vec{e}p\to e\gamma p} = \sigma_{BH} + e_\ell \sigma_{INT} + P_\ell e_\ell \tilde{\sigma}_{INT} + \sigma_{VCS} + P_\ell \tilde{\sigma}_{VCS} \tag{6}$$

where σ is even in azimuthal angle ϕ, and $\tilde{\sigma}$ is odd in ϕ. The interference terms $\sigma_{INT} \sim \mathrm{Re}A_{\gamma^*\mathrm{N}\to\gamma\mathrm{N}}$ and $\tilde{\sigma}_{INT} \sim \mathrm{Im}A_{\gamma^*\mathrm{N}\to\gamma\mathrm{N}}$ are the real and imaginary parts, respectively of the Compton amplitude. Using polarized electrons the combination $-\tilde{\sigma}_{INT}+\tilde{\sigma}_{VCS}$ can be determined by taking the difference of the beam helicities. The electron-positron charge difference for unpolarized beams determines σ_{INT}. For fixed beam polarization and taking the electron-positron difference one can extract the combination $P_\ell\tilde{\sigma}_{INT} + \sigma_{INT}$. If only a polarized electron beam is available one can separate $\tilde{\sigma}_{INT}$ from $\tilde{\sigma}_{VCS}$ using the Rosenbluth technique [16]. This requires measurements at two significantly different beam energies which reduces the kinematical coverage that can be achieved with this method. With polarized electrons and polarized positrons both σ_{INT} can be determined and $\tilde{\sigma}_{INT}$ can be separated from $\tilde{\sigma}_{VCS}$ in the full kinematic range available at the maximum beam energy.

Differential cross section for polarized proton target

The structure of the differential cross section for polarized beam and polarized target contains the polarized beam term of the previous section and an additional term related to the target polarization [19, 20]:

$$\sigma_{\vec{e}\vec{p}\to e\gamma p} = \sigma_{\vec{e}p\to e\gamma p} + T[P_\ell \Delta\sigma_{BH} + e_\ell \Delta\tilde{\sigma}_{INT} + P_\ell e_\ell \Delta\sigma_{INT} + \Delta\tilde{\sigma}_{VCS} + P_\ell \Delta\sigma_{VCS}] \tag{7}$$

where the target polarization T can be longitudinal or transverse. If only unpolarized electrons are available, the combination $-\Delta\tilde{\sigma}_{INT}+\Delta\tilde{\sigma}_{VCS}$ can be measured from the differences in the target polarizations. If unpolarized electrons and unpolarized positrons are available the combination $T\Delta\tilde{\sigma}_{INT}+\sigma_{INT}$ can be determined at fixed target polarization. With both polarized electron and polarized positron beams, the combination $T\Delta\tilde{\sigma}_{INT} + TP_\ell\Delta\sigma_{INT} + P_\ell\tilde{\sigma}_{INT} + \sigma_{INT}$ can be measured at fixed target polarization. Availability of both polarized electron and polarized positron beams thus allows the separation of all contributing terms. If only polarized electron beams are available a Rosenbluth separation with different beam energies can separate the term $\Delta\tilde{\sigma}_{INT}$ from $\Delta\tilde{\sigma}_{VCS}$, again in a much more limited kinematical range and with likely larger systematic uncertainties. The important interference term $\Delta\sigma_{INT}$ can only be determined using the combination of polarized electron and polarized positron beams.

ESTIMATES OF EXPERIMENTAL UNCERTAINTIES

The CLAS12 Detector

The experimental program will use the CLAS12 detector, shown in Fig. 2, for the detection of the hadronic final states. CLAS12 consists of a Forward Detector (FD) and a Central Detector (CD). The Forward Detector is comprised of six symmetrically arranged sectors defined by the six coils of the superconducting torus magnet. Charged particle tracking is provided by a set of 18 drift chambers with a total of 36 layers in each sector. Additional tracking at $5^\circ - 35^\circ$ is achieved by a set of 6 layers of micromesh gas detectors (micromegas) immediately downstream of the target area and in front of the High Threshold Cherenkov Counter (HTCC). Particle identification is provided by time-of-flight information from two layers of scintillation counter detectors (FTOF). Electron, photon, and neutron detection are provided by the triple layer electromagnetic calorimeter, PCAL, EC(inner), and EC(outer). The heavy-gas Cherenkov Counter (LTCC) provides separation of high momentum pions from kaons and protons. The Central Detector consists of 6 to 8 layers (depending on the configuration) of silicon strip detectors with stereo readout and 6 layers of micromegas arranged as a barrel around the target, a barrel of scintillation counters to measure the particle flight time from the target (CTOF), and a scintillation-counter based Central Neutron Detector (CND).

Beam spin asymmetries on protons

Beam spin asymmetries of polarized electrons for the DVCS process have been measured at lower energies and are known to be large, up to

$$A_e \equiv \frac{\sigma^+ - \sigma^-}{\sigma^+ - \sigma^-} = 0.3 - 0.4\ ,$$

where σ^+ and σ^- are the cross sections for the electron beam spin parallel and spin anti-parallel to the electron beam direction. Figure 3 shows projections of the beam asymmetry for some specific kinematics at an electron beam energy of 11 GeV. The uncertainties are are estimated assuming an experiment of 1000 hrs at an instantaneous luminosity of $L = 10^{35}\text{cm}^2\text{s}^{-1}$. The asymmetry is the results of the interference term $\tilde{\sigma}_{INT}$ in equation (6). Note that the magnitude of the interference is independent of the electric charge, but the sign of the asymmetry is opposite for electrons and positrons.

Equation (6) also shows that the term σ_{INT} can be isolated in the difference of unpolarized electrons and positrons. Examples of the charge difference and the charge asymmetry are shown in Figure 4. The unpolarized charge asymmetry A_c^{UU} and its $\cos\phi$ moment $A^{\cos\phi}$ can both be large for the dual model assumed in our estimate.

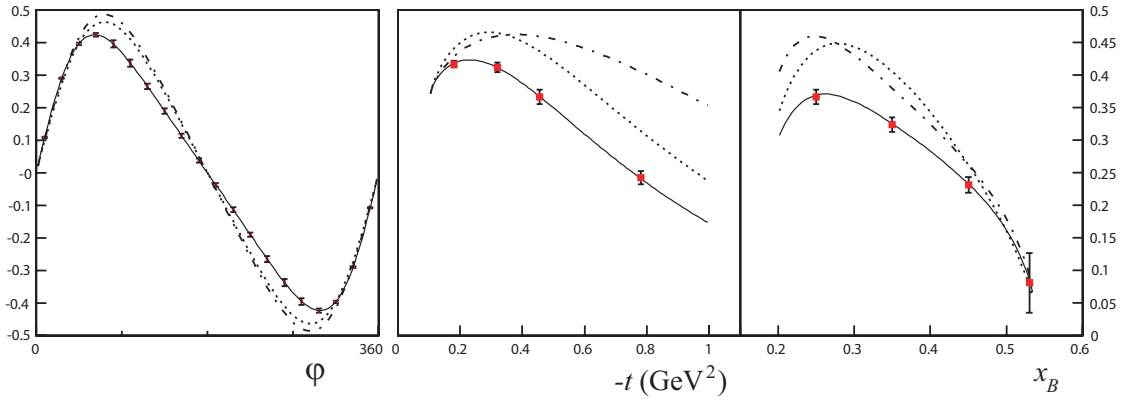

FIGURE 3. The beam spin asymmetry showing the DVCS-BH interference for 11 GeV beam energy [17]. Left panel: $x = 0.2$, $Q^2 = 3.3\text{GeV}^2$, $-t = 0.45\text{GeV}^2$. Middle and right panels: $\phi = 90^\circ$, other parameters same as in left panel. Many other bins will be measured simultaneously. The curves represent various parameterizations within the VGG model [18]. Projected uncertainties are statistical.

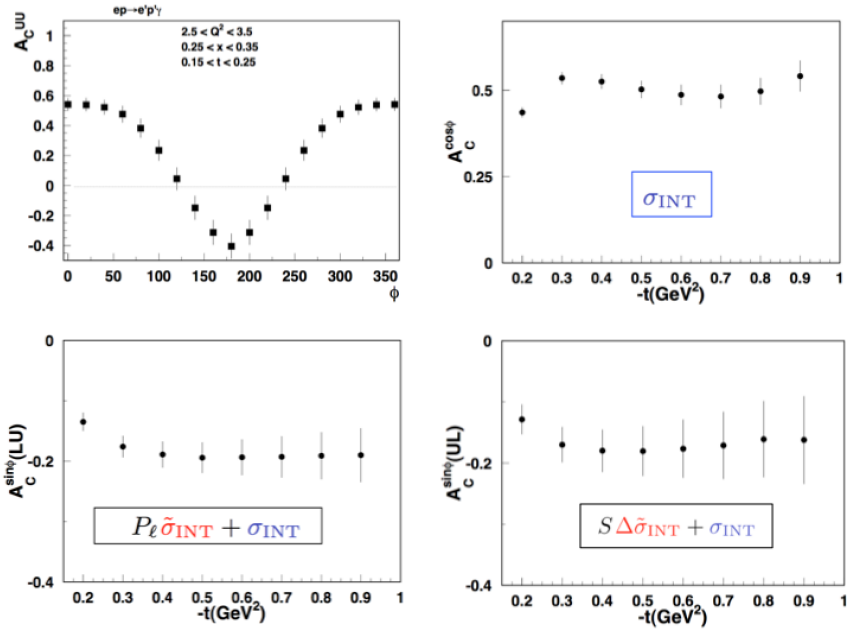

FIGURE 4. Electron-positron DVCS charge asymmetries: Top-left: Azimuthal dependence of the charge asymmetry for positron and electron beam at 11 GeV beam. Top-right: Moment in cos(ϕ) of the charge asymmetry versus momentum transfer t to the proton. Bottom-left: Charge asymmetries for polarized electron and positron beams at fixed polarization (LU). Bottom right: Charge asymmetry for longitudinally polarized protons at fixed polarization (UL). The error bars are estimated for a 1000 hrs run with positron beam and luminosity $L = 2\times10^{34}$ cm^{-2}sec^{-1} at a beam polarization $P = 0.6$. Electron luminosity $L = 10\times10^{34}$ cm^{-2}sec^{-1}, and electron beam polarization $P = 0.8$. The error bars are statistical for a single bin in Q^2, x, and t as shown in the top-left panel. Other bins are measured simultaneously.

Estimates of charge asymmetries for different lepton charges

For quantitative estimates of the charge differences in the cross sections we use the acceptance and luminosity achievable with CLAS12 as basis for measuring the process $ep \rightarrow e\gamma p$ at different beam and target conditions. A 5 cm long liquid hydrogen is assumed with an electron current of 75nA, corresponding to an operating luminosity of 10^{35}cm^{-2}sec^{-1}. For the positron beam a 5 times lower beam current of 15nA is assumed. In either case 1000 hours of beam time is used for the rate projections. For quantitative estimates of the cross sections the dual model [21, 22] is used. It incorporates parameterizations of the GPDs H and E. As shown in Fig. 4, effects coming from the charge asymmetry can be large. In case of unpolarized beam and unpolarized target the cross section for electron scattering has only a small dependence on azimuthal angle ϕ, while the corresponding positron cross section has a large ϕ modulation. The difference is directly related to the term σ_{INT} in equation (6).

The Science Case for DVCS with polarized Positrons

In previous sections we have shown that polarized positron beams are necessary to disentangle all contributions to the The science program for DVCS with electrons beams has been well established, and several approved experiments for 12 GeV operation have already been carried out or are currently in the process and planned for the next few years. What do polarized positron beams add that makes a most compelling case for the developing of a polarized positron beam for experiments with CLAS12? In this section we discuss on one example what the impact of DVCS measurements with polarized positron beams can bring to the unraveling the force distribution on quarks in the proton. Here we refer to the recent publication in the journal Nature of the results of an analysis on the pressure distribution in the proton [23].

The Nature paper is based on the results of Beam Spin Asymmetry and Unpolarized Cross-Section DVCS mea-

surements performed with CLAS in Hall B. The determination of the pressure distribution proceeds in several steps:

- We begin with the sum rules that relate the second Mellin moments of the GPDs to the Gravitational Form Factors (GFFs) [26].
- We then define the complex CFF $\mathcal{H}$, which is directly related to the experimental observables describing the DVCS process, i.e., the differential cross section and the beam spin asymmetry.
- The real and imaginary parts of $\mathcal{H}$ can be related through a dispersion relation [39, 40, 41] at fixed t, where the $D(t)$-term appears as a subtraction constant [42].
- We recover $d_1(t)$ from the expansion of the $D(t)$-term in the Gegenbauer polynomials of ξ, the momentum transfer to the struck quark.
- We finally proceed with the fits to the data and extract $D(t)$ and determine $d_1(t)$.
- The pressure distribution is then determined from the relation of $d_1(t)$ and $p(r)$ through a Bessel integral.

The sum rules that relate the second Mellin moments of the chiral-even GPDs to the GFFs are [26]:

$$\begin{aligned}\int \mathrm{d}x\, x\left[H(x,\xi,t)+E(x,\xi,t)\right] &= 2J(t)\\ \int \mathrm{d}x\, xH(x,\xi,t) &= M_2(t)+\frac{4}{5}\xi^2 d_1(t),\end{aligned}$$

where $M_2(t)$ and $J(t)$ respectively correspond to the time-time and time-space components of the Energy Momentum Tensor (EMT), and give access to the mass and total angular momentum distributions carried by the quarks in the proton, and where the quantity $d_1(t)$ corresponds to the space-space components of the EMT, and encodes the shear forces and pressure acting on the quarks. We have some constraints on $M_2(t)$ and $J(t)$, notably at $t = 0$ they are fixed to the proton's mass and spin. By contrast, almost nothing is known on the equally fundamental quantity $d_1(t)$. As the GFF $d_1(t)$ encodes the shear forces on the quarks and pressure distribution in the proton, we can expect the existence of a zero sum rule ensuring the total pressure and forces to vanish, thus preserving the stability of the dynamics. The observables are parameterized by the CFFs, which for the GPD H are the real quantities Re$\mathcal{H}$ and Im$\mathcal{H}$ defined by :

$$\mathrm{Re}\mathcal{H}(\xi,t)+i\mathrm{Im}\mathcal{H}(\xi,t)=\int_{-1}^{1}dx\left[\frac{1}{\xi-x-i\epsilon}-\frac{1}{\xi+x-i\epsilon}\right]H(x,\xi,t) \tag{8}$$

The average quark momentum fraction x is not observable in the process; it is integrated over with the quark propagators. Analytical properties of the amplitude in the Leading Order (LO) approximation lead to the dispersion relation :

$$\mathrm{Re}\mathcal{H}(\xi,t)\overset{\mathrm{LO}}{=}D(t)+\frac{1}{\pi}\mathcal{P}\int_0^1 dx\left(\frac{1}{\xi-x}-\frac{1}{\xi+x}\right)\mathrm{Im}\mathcal{H}(x,t) \tag{9}$$

where the subtraction constant is the so-called D-term. The dispersion relation allows us trading-off the two CFFs as unknowns with one CFF and the D-term [43, 44].

For our purpose we recover the $d_1(t)$ as the first coefficient in the Gegenbauer expansion of the D-term. Here, we will truncate this expansion to $d_1(t)$ only.

$$D(t)=\frac{1}{2}\int_{-1}^{1}\mathrm{d}z\frac{D(z,t)}{1-\mathrm{z}} \tag{10}$$

with

$$D(z,t)=(1-z^2)\left[d_1(t)C_1^{3/2}(z)+\cdots\right] \tag{11}$$

and

$$-1<z=\frac{x}{\xi}<1 \tag{12}$$

Our starting points in the analysis are the global fits presented in [35, 36], referred to as KM parameterization. The imaginary part of the amplitude is calculated from a parameterization of the GPDs along the diagonal $x = \xi$. The real part of the amplitude is then reconstructed assuming LO dominance and applying the dispersion relation. The ξ-dependence of the D-term is completely generated by the Gegenbauer expansion, restricted to the $d_1(t)$ term only. Finally, the momentum transfer dependence of the $d_1(t)$ term is given as a functional form, with three parameters $d_1(0)$, M, and α :

$$d_1(t)=d_1(0)\left(1-\frac{t}{M^2}\right)^{-\alpha}, \tag{13}$$

where the chosen form of $d_1(t)$ with $\alpha = 3$ is consistent with the asymptotic behavior required by the dimensional counting rules in QCD [45]. We adjust and fix the central values of the model parameters to the data at 6 GeV [34, 33]. They include unpolarized and polarized beam cross-sections over a wide phase-space in the valence region, and support the model indicating that the GPD H largely dominates these observables. An illustration of a fit to the $d_1(t)$ dependence is provided in figure 14. The data points correspond to the values extracted from the fit to the unpolarized cross section data in figure 3. The experimental analysis shows that $d_1(0)$ has a negative sign. This is consistent with several theoretical studies [48, 47, 41]. The fit results in a $d_1(0)$ value of:

$$d_1(0) = -2.04 \pm 0.14(\text{stat.}) \pm 0.33(\text{syst.}).$$

The negative sign of $d_1(0)$ found in this analysis seems deeply rooted in the spontaneous breakdown of chiral symmetry [46], which is a consequence of the transition of the microsecond old universe from its state of de-confined quarks and gluons to the state of confined quarks in stable protons. It is thus intimately connected to the stability of the proton [48] and of the visible universe.

We finally can relate the GFF $d_1(t)$ to the pressure distribution *via* the spherical Bessel integral :

$$d_1(t) \propto \int \mathrm{d}^3\mathbf{r}\, \frac{\mathrm{j}_0(\mathrm{r}\sqrt{-t})}{2t}\, \mathrm{p(r)} \tag{14}$$

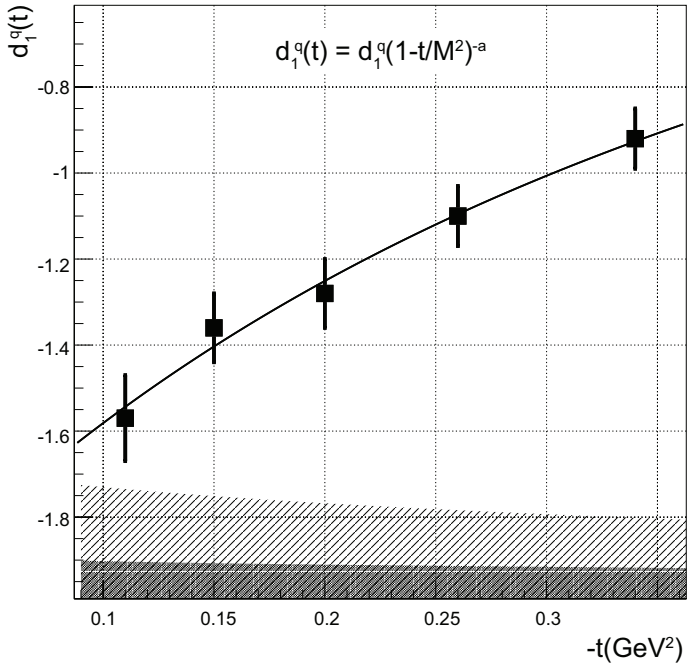

FIGURE 5. Example of a fit to $d_1(t)$. The error bars are from the fit to the cross sections at fixed value of $-t$. The single-shaded area at the bottom corresponds to the uncertainties from the extension of the fit into regions without data and is reflected in the green shaded are in Fig. 6. The double-shaded area corresponds with the projected uncertainties from future experiment [49] as shown in Fig. 6 with the red shaded area. Uncertainties represent 1 standard gaussian deviation.

Our results on the quark pressure distribution in the proton are illustrated in figure 6. The black central line corresponds to pressure distribution $r^2p(r)$ extracted from the D-term parameters fitted to the published data at 6 GeV [34].The corresponding estimated uncertainties are displayed as the shaded area shown in light green. There is a positive core and a negative tail of the $r^2p(r)$ distribution as a function of the radial distance from the proton's center with a zero-crossing near 0.6 fm from that center. We also note that the regions where repulsive and binding pressures dominate are separated in radial space, with the repulsive distribution peaking near $r = 0.25$ fm, and the maximum of the negative pressure responsible for the binding occurring near $r = 0.8$ fm. The outer shaded area shown in dark green in figure 1 corresponds with the D-term uncertainties obtained in the global fit results from previous research [35, 36].

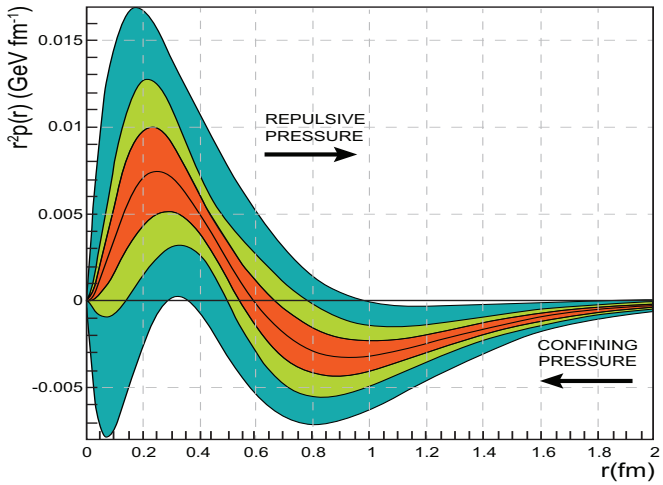

FIGURE 6. The radial pressure distribution in the proton. The graph shows the pressure distribution $r^2 p(r)$ resulting from the interactions of the quarks in the proton versus the radial distance from the center in femtometer. The black central line corresponds to the pressure extracted from the D-term parameters fitted to the published data at 6 GeV [34]. The corresponding estimated uncertainties are displayed as the shaded area shown in light green. Uncertainties represent 1 standard deviation.

They exhibit a shape similar to the light green area and confirm the robustness of the analysis procedure to extract the D-term. Here we remark that the pressure $p(r)$ must satisfy the stability condition

$$\int_0^\infty r^2 p(r) dr = 0, \tag{15}$$

which is realized within the uncertainties of our analysis. The shape of the radial pressure distribution mimics closely the results obtained within the chiral quark soliton model [48]. In this model, the proton is modeled as a chiral soliton in which constituent quarks are bound by a self-consistent pion field. The comparison with our results suggests that the pion field is significantly relevant for the description of the proton as a bound state of quarks.

What positrons will add to this program

There a couple of limiting factors in the analyses presented above. These are related to the limited experimental information that can be obtained from having just polarized electron baem available. The details of the limiting factors were discussed section a) and in subsection a), and in subsection a).

- The use of the dispersion relation in equ. (9) to determine the Re$\mathcal{H}(\xi, t)$
- The need to extrapolate the $t-$dependence of the formula in equ. (14).

While the extrapolation is unavoidable when extracting the pressure distribution over the entire radial distance, applying the dispersion relation in equ.(9) at large $-t$ values is problematic where issues with convergence may occur. It is therefore highly desirable to determine the subtraction term $D(t)$ directly from the DVCS data without the need for applying the dispersion relation. Such a procedure requires to determine both, the imaginary part of CFF $\mathcal{H}(\xi, t)$ in equ. (9) directly from experiment. The term $D(t)$ can then be directly extracted. By isolating the terms σ_{INT} and the term $\bar{\sigma}_{INT}$ in equ. (6), we can separate the real and imaginary parts of the Compton amplitude. The separation can by achieved by measuring the difference in the unpolarized cross sections and the helicity-dependent cross sections for (polarized) electrons and (polarized) positrons. From figure 4 we can infer that both of these observables can result in large cross section differences and polarization asymmetries, and can be well measured already with modest positron currents, by making use of the large acceptance capabilities of CLAS12.

While our focus for this LOI is the determination of the pressure distribution and the shear forces in the proton (and neutron), using a spin polarized target and and polarized electron and positrons we can separate the term $\Delta\sigma_{INT}$ in equ. (7) which is related to the GPD E in equ. (4) and corresponding Compton form factor $\mathcal{E}(\xi, t)$. These quantities

are related to the angular momentum distribution in the proton. Measurement of $\mathcal{E}(\xi, t)$ will allow for the extraction of the radial dependence of the angular momentum density in protons and can be determined in a fashion similar to the one described for the pressure distribution.

Experimental Setup for DVCS Experiments

Figure 7 shows generically how the electron-proton and the positron-proton DVCS experiments would be configured. Electrons and positrons will be detected in the forward detection system of CLAS12. However, for the positron run the Torus magnet would have the reversed polarity so that positron trajectories would look identical to the electron trajectories in the electron-proton experiment, and limit systematic effects in acceptances. The recoil proton in both cases would be detected in the Central Detector at the same solenoid magnet polarity, also eliminating most systematic effects in the acceptances. However, there is a remaining systematic difference in the two configuration, as the forward scattered electron/positron would experience different transverse field components in the solenoid, which will cause the opposite azimuthal motion in ϕ in the forward detector. A good understanding of the acceptances in both cases is therefore important. The high-energy photon is, of course, not affected by the magnetic field configuration.

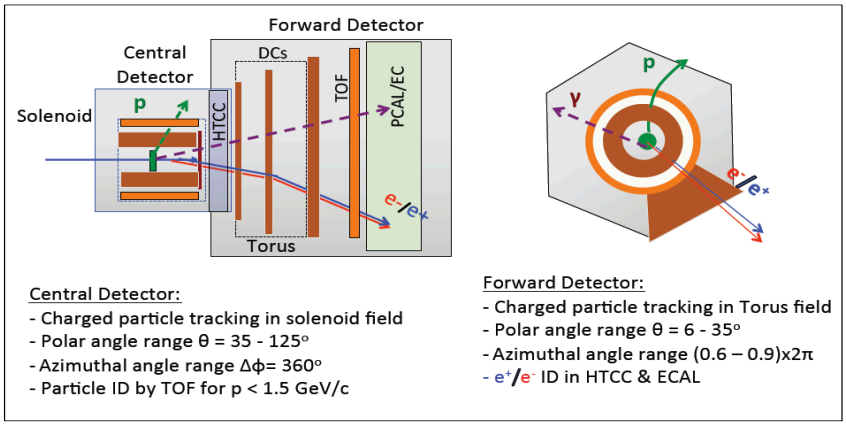

FIGURE 7. Generic CLAS12 configuration for the electron-proton and the positron-proton experiments. The central detector will detect the protons, and the bending in the magnetic solenoid field will be identical for the same kinematics. The electron and the positron, as well as the high-energy DVCS photon will be detected in the forward detector part. The electron and positron will be deflected in the Torus magnetic field in the same way as the Torus field direction will be opposite in the two experiments. The deflection in ϕ due to the solenoid fringe field will be of same magnitude $\Delta\phi$ but opposite in direction. The systematic of this shift can be controlled by doing the same experiment with opposite solenoid field directions that would result in the sign change of the $\Delta\phi$.

Conclusions

In this LOI we described the use of a new polarized positron beam in conjunction with the already available polarized electron beam to significantly enhance the program to study the generalized parton distribution and to extract physical quantities that are related to the mechanical properties of the proton, such as the distribution of shear forces, the pressure distribution, mechanical radius of the proton, and angular momentum distribution. These quantities have never before been measured as they couple directly only to the gravitational field. The development of the generalized parton distributions and their relation ship to the gravitational form factors through the second Mellin moments made this feasible in an indirect way. First results have been obtained recently [23]. An experiment has been approved by PAC44 using a polarized electron beam to improved the precision of the pressure distribution. The use of the CLAS12 detector to broaden this program is natural as the expected polarized positron current is much lower than what can be achieved with polarized electron beams, and fits naturally with the capabilities of the CLAS12. Simulations have been

made with realistic beam currents and beam polarization that show that the relevant observables can be measured with good accuracy and will have a very significant impact and the scientific results.

Acknowledgment

REFERENCES

[1] M. Diehl, Phys. Rept. **388**, 41 (2003) [hep-ph/0307382].
[2] A. V. Belitsky and A. V. Radyushkin, Phys. Rept. **418**, 1 (2005) [hep-ph/0504030].
[3] A. V. Belitsky, X. d. Ji and F. Yuan, Phys. Rev. D **69**, 074014 (2004) [hep-ph/0307383].
[4] X. d. Ji, Phys. Rev. Lett. **91**, 062001 (2003) [hep-ph/0304037].
[5] M. Burkardt, Int. J. Mod. Phys. A **18**, 173 (2003) [hep-ph/0207047].
[6] H. S. Jo *et al.* [CLAS Collaboration], Phys. Rev. Lett. **115**, no. 21, 212003 (2015) [arXiv:1504.02009].
[7] G. Gavalian *et al.* [CLAS Collaboration], Phys. Rev. C **80**, 035206 (2009) [arXiv:0812.2950 [hep-ex]].
[8] F. X. Girod *et al.* [CLAS Collaboration], Phys. Rev. Lett. **100**, 162002 (2008) [arXiv:0711.4805 [hep-ex]].
[9] C. M. Camacho *et al.* [Jefferson Lab Hall A], Phys. Rev. Lett. **97**, 262002 (2006) [nucl-ex/0607029].
[10] S. Stepanyan *et al.* [CLAS Collaboration], Phys. Rev. Lett. **87**, 182002 (2001) [hep-ex/0107043].
[11] S. Pisano *et al.* [CLAS Collaboration], Phys. Rev. D **91**, no. 5, 052014 (2015) [arXiv:1501.07052 [hep-ex]].
[12] E. Seder *et al.* [CLAS Collaboration], Phys. Rev. Lett. **114**, no. 3, 032001 (2015) Addendum: [Phys. Rev. Lett. **114**, no. 8, 089901 (2015)] [arXiv:1410.6615 [hep-ex]].
[13] S. Chen *et al.* [CLAS Collaboration], Phys. Rev. Lett. **97**, 072002 (2006) [hep-ex/0605012].
[14] M. Guidal, H. Moutarde and M. Vanderhaeghen, Rept. Prog. Phys. **76**, 066202 (2013) [arXiv:1303.6600].
[15] K. Kumericki and D. Mueller, arXiv:1205.6967 [hep-ph].
[16] M. N. Rosenbluth, Phys. Rev. **79**, 615 (1950).
[17] JLab experiment E12-06-119, F. Sabatie et al. (spokespersons).
[18] M. Vanderhaeghen, P. A. M. Guichon and M. Guidal, Phys. Rev. D **60**, 094017 (1999) [hep-ph/9905372].
[19] A. V. Belitsky, D. Mueller and A. Kirchner, Nucl. Phys. B **629**, 323 (2002) [hep-ph/0112108].
[20] M. Diehl and S. Sapeta, Eur. Phys. J. C **41**, 515 (2005) [hep-ph/0503023].
[21] V. Guzey and T. Teckentrup, Phys. Rev. D **79**, 017501 (2009) [arXiv:0810.3899 [hep-ph]].
[22] V. Guzey and T. Teckentrup, Phys. Rev. D **74**, 054027 (2006) [hep-ph/0607099].
[23] V.D. Burkert, L. Elouadrhiri, F.X. Girod, Nature **557**, 396399 (2018).
[24] Ozel, F. & Freire, P. "Masses, Radii, and Equation of State of Neutron Stars", Ann. Rev. Astron. Astrophys. **54**, 401-440 (2016).
[25] Pagels, H. "Energy-Momentum Structure Form Factors of Particles", Phys. Rev. **144**, 1250-1260 (1966).
[26] Ji, X. D. "Deeply virtual Compton scattering", Phys. Rev. D **55**, 7114-7125 (1997).
[27] Teryaev, O. V. "Gravitational form factors and nucleon spin structure", Front. Phys. (Beijing) **11**, 111207 - 111207-8 (2016)
[28] Belitsky, A. V., & Radyushkin, A. V. "Unraveling hadron structure with generalized parton distributions", Phys. Rept. **418**, 1-387 (2005)
[29] Müller, D., Robaschik, D., Geyer, D., Dittes, F.M., & Hořejši, J. "Wave functions, evolution equations and evolution kernels from light ray operators of QCD", Fortsch. Phys. **42**, 101-141 (1994)
[30] Ji, X. D. "Gauge-Invariant Decomposition of Nucleon Spin", Phys. Rev. Lett. **78**, 610-613 (1997)
[31] Radyushkin, A. V. "Scaling limit of deeply virtual Compton scattering", Phys. Lett. B **380**, 417-425 (1996)
[32] Polyakov, M. V. "Generalized parton distributions and strong forces inside nucleons and nuclei", Phys. Lett. B **555**, 57-62 (2003)
[33] Girod, F. X *et al.* [CLAS Collaboration], "Measurement of Deeply virtual Compton scattering beam-spin asymmetries", Phys. Rev. Lett. **100**, 162002 (2008)
[34] Jo, H. S. *et al.* [CLAS Collaboration], "Cross sections for the exclusive photon electroproduction on the proton and Generalized Parton Distributions", Phys. Rev. Lett. **115**, no. 21, 212003 (2015).
[35] Kumerički, K., & Müller, D. "Deeply virtual Compton scattering at small x_B and the access to the GPD H", Nucl. Phys. B **841**, 1-58 (2010)
[36] Müller, D., Lautenschlager, T., Passek-Kumericki, K., & Schaefer, A. "Towards a fitting procedure to deeply virtual meson production - the next-to-leading order case", Nucl. Phys. B **884** (2014) 438-546

[37] Guidal, M., Moutarde, H., & Vanderhaeghen, M. "Generalized Parton Distributions in the valence region from Deeply Virtual Compton Scattering", Rept. Prog. Phys. **76**, 066202 (2013)

[38] Kumericki, K., Liuti, S., & Moutarde, H. "GPD phenomenology and DVCS fitting : Entering the high-precision era", Eur. Phys. J. A **52**, no. 6, 157 (2016)

[39] Diehl, M., & Ivanov, D. Y. "Dispersion representations for hard exclusive processes: beyond the Born approximation", Eur. Phys. J. C **52**, 919-932 (2007)

[40] Anikin, I. V., & Teryaev, O. V. "Dispersion relations and QCD factorization in hard reactions", Fizika B **17**, 151-158 (2008)

[41] Pasquini, B., Polyakov, M. V., & Vanderhaeghen, M. "Dispersive evaluation of the D-term form factor in deeply virtual Compton scattering", Phys. Lett. B **739**, 133-138 (2014)

[42] Polyakov, M. V., & C. Weiss, "Skewed and double distributions in pion and nucleon", Phys. Rev. D **60**, 114017 (1999)

[43] Radyushkin, A. V. "Modeling Nucleon Generalized Parton Distributions", Phys. Rev. D **87**, 096017 (2013)

[44] Radyushkin, A. V. "Sum rules for nucleon generalized parton distributions and border function formulation", Phys. Rev. D **88**, 056010 (2013)

[45] Lepage, G. P., & Brodsky, S. J. "Exclusive Processes in Perturbative Quantum Chromodynamics", Phys. Rev. D **22**, 2157-2314 (1980).

[46] Kivel, N., Polyakov, M. V., and Vanderhaeghen, M. "DVCS on the nucleon: Study of the twist - three effects," Phys. Rev. D **63**, 114014 (2001)

[47] Kim, H. C., Schweitzer, P., & Yakhshiev, U. "Energy-momentum tensor form factors of the nucleon in nuclear matter", Phys. Lett. B **718**, 625-631 (2012)

[48] Goeke, K., Grabis, J., Ossmann, J., Polyakov, M. V., Schweitzer, P., Silva, A., & Urbano, D. "Nucleon form-factors of the energy momentum tensor in the chiral quark-soliton model", Phys. Rev. D **75**, 094021 (2007)

[49] Elouadrhiri, L. *et al.* [CLAS Collaboration], 'Deeply Virtual Compton Scattering with CLAS12 at 6.6 GeV and 8.8 GeV", E12-16-010B approved by Jefferson Lab PAC44

[50] M. I. Eides, V. Y. Petrov and M. V. Polyakov, "Narrow Nucleon-$\psi(2S)$ Bound State and LHCb Pentaquarks," Phys. Rev. D **93**, no. 5, 054039 (2016)

[51] Jung, J.H., Yakhshiev, U., Kim, H. C., & Schweitzer, P. "In-medium modified energy-momentum tensor form factors of the nucleon within the framework of a π-ρ-ω soliton model", Phys. Rev. D **89**, 114021 (2014)

[52] I. A. Perevalova, M. V. Polyakov and P. Schweitzer, "On LHCb pentaquarks as a baryon-ψ(2S) bound state: prediction of isospin-$\frac{3}{2}$ pentaquarks with hidden charm," Phys. Rev. D **94**, no. 5, 054024 (2016)

[53] J. Hudson and P. Schweitzer, "D term and the structure of pointlike and composed spin-0 particles," Phys. Rev. D **96**, no. 11, 114013 (2017